ACS Sustainable Chemistry & Engineering

Research Article

pubs.acs.org/journal/ascecg

Novel Magnetite Nanoparticles Coated with Waste-Sourced Biobased Substances as Sustainable and Renewable Adsorbing Materials

Giuliana Magnacca,[†] Alex Allera,[†] Enzo Montoneri,[†] Luisella Celi,[‡] Damián E. Benito,[§] Leonardo G. Gagliardi,[§] Mónica C. Gonzalez,[∥] Daniel O. Mártire,[∥] and Luciano Carlos*[,∥]

[†]Dipartimento di Chimica, Università di Torino, Via Giuria 7, Torino, Italy

[‡]Università di Torino, DISAFA, via L. da Vinci 44, Grugliasco, Italy

[§]LIDMA, Universidad Nacional de La Plata, Calle 1 y 47, La Plata, Argentina

[∥]Instituto de Investigaciones Fisicoquímicas Teóricas y Aplicadas (INIFTA), CCT-La Plata-CONICET, Universidad Nacional de La Plata, Diag 113 y 64, La Plata, Argentina

S *Supporting Information*

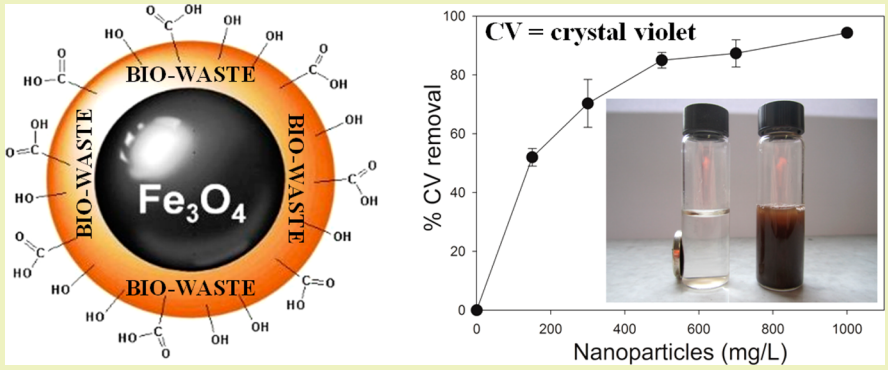

ABSTRACT: This study examines the possibility of using a biobased product isolated from urban solid wastes as a material for environmental technological applications. To this end, Fe_3O_4 nanoparticles (NPs) coated with different amounts of soluble biobased products (SBO) were synthesized as a low-cost nanoadsorbent for the removal of pollutants in wastewater. Particles of 10 nm diameter with an Fe_3O_4 core and SBO shell were obtained. The concentration of SBO employed in the synthesis had no effect on the size and structure of the NPs but ruled the pH_{PZC} and aggregation of the nanoparticles in water. The cationic dye crystal violet (CV) was used as a model pollutant to test the adsorption capacity of the nanoparticles. The results indicated that both the medium pH and NP dosage were significant parameters to enhance the removal of CV. The results contribute to the studies that show how wastes can become a source of revenue through the industrial exploitation of their chemical value.

KEYWORDS: *Nanoadsorbents, Magnetite, Wastewater remediation, Urban biowastes, Renewable feedstock, Crystal violet*

INTRODUCTION

Not always are the conventional wastewater treatments effective in the removal of pollutants from wastewater, in particular when pollutants belong to several classes and possess different behaviors. In cases like these, further treatments need to be exploited. The aim of this study is to investigate unusual materials as adsorbents in order to act together and/or assist other abatement techniques.[1] Adsorbent materials present also the advantage to avoid the appearance of secondary pollution (due to the application of traditional degradative methods that can lead to the formation of toxic intermediates).

In recent years, a wide number of publications have been dedicated to the removal of pollutants from wastewater by using adsorption techniques. One of the most important requirements to keep in mind during the development of these strategies is the cost of the technologies proposed, which needs to be very limited. In this respect, low-cost materials from natural sources (natural clay minerals like montmorillonite, bentonite, sepiolite, vermiculite, and zeolites), industrial wastes (such as fly ash, blast furnace slag and sludge, black liquor lignin, red mud, and waste slurry), and agriculture residues have been considered.[2−7] Adsorbents deriving from agricultural operations, in particular, deserve a careful evaluation, because they are available in large quantities, are environmentally friendly, and have almost no costs.[8] In this context, the use of substances deriving from treatment of biowastes (green

Received: March 25, 2014
Revised: May 9, 2014
Published: May 13, 2014

disposal and food) represents a good contribution to this research, and to our best knowledge, solid urban wastes (or byproducts) have never been tested as low-cost adsorbents. Recent research has shown that the recalcitrant lignin-like fraction of urban solid wastes is a cost-effective source of soluble biobased products (SBO) that can be rather effective in a wide number of applications in the industry and environmental remediation.[9−12] SBO have been found to be mixtures of molecules differing in molecular weight (from 67 to 463 kg mol^{-1}) that are composed of aliphatic C chains substituted by aromatic rings and several functional groups such as COOH, CON, CO, PhOH, and O-alkyl among others.[13] Their potential use as adsorbent material for removal of pollutants from wastewater could be useful from a number of perspectives because it could contribute to reduce the environmental impact of urban wastes, and it may revalorize solid urban wastes as a material of technological application.

This work takes inspiration from the preparation of magnetic materials using humic substances as an active adsorbing phase,[14] extending the study to the use of SBO extracted from wastes following an already optimized procedure.[15] In fact, in recent years, nanoscale iron oxides have attracted growing interest in water treatment and environmental remediation. In particular, the use of magnetite nanoparticles as adsorbents in water treatment provides a convenient approach for separating and removing the contaminants by applying external magnetic fields. Because bare magnetite nanoparticles are susceptible to air oxidation and are easily aggregated in aqueous systems,[16] their surface modifications are commonly performed for application as nanoadsorbents.[17−19]

The present paper reports the preparation of Fe_3O_4 nanoparticles (NPs) coated with SBO as low-cost nanoadsorbents for removal of pollutants in wastewater. The physical and chemical characterization of the synthesized SBO-coated Fe_3O_4 nanoparticles was carried out.

Dye molecules when released to wastewaters cause serious environmental and health hazards.[20] In particular, the cationic azo dye crystal violet (CV) is considered a mitotic poison.[21] For these reasons and with the aim of developing a method for the removal of CV from waters, the sorption capacity of the SBO-coated Fe_3O_4 nanoparticles for adsorbing the hazardous dye CV was tested, and the effects of pH, ionic strength, and NP dosages were evaluated.

EXPERIMENTAL SECTION

Synthesis. The coated magnetite nanoparticles were prepared by modifying the coprecipitation method in the presence of a suitable concentration of SBO. First, 3.7 g of $FeCl_3$ and 4.2 g of $FeSO_4 \times 7H_2O$ were dissolved in 100 mL of deionized water. The solution was brought to 90 °C and then 10 mL of NH_4OH 25% and 50 mL of solution containing various amounts of SBO (0.05, 0.1, and 0.5 g) were sequentially added. The solution was kept at 90 °C for 30 min under continuous stirring and was subsequently cooled to room temperature. The magnetic powder was separated from the basic solution using a laboratory magnet and was washed three times with water in order to eliminate all the undesired soluble and nonmagnetic products. Finally, the black powders were dried in a vacuum oven at 70 °C for several hours and then stored at room temperature. Depending on the amount of SBO used during the synthesis (0.05, 0.1, and 0.5 g), the samples were named as NP/0.05, NP/0.1, and NP/0.5, respectively.

All commercial products used were purchased from Sigma-Aldrich. The SBO employed in this study, namely, CVT230, was derived from 230 days of composting of green refuse (at Acea Pinerolese plant at Pinerolo, Torino, Italy) and was processed at the pilot plant of Studio Chiono e Associati at Rivarolo Canavese, Torino, Italy. The extraction procedure of CVT230 as well as its physicochemical characterization was already reported elsewhere.[11,22]

Characterization. Magnetization measurements were carried out with a LakeShore 7404 vibrating sample magnetometer. The hysteresis loop of the samples was registered at room temperature (25 °C) as the magnetic field was cycled between −2 and 2 kOe. Nitrogen adsorption at 77 K was followed using a gas volumetric apparatus ASAP2020 by Micrometrics to determine specific surface area and porosity. Samples were pretreated for several hours at 70 °C in order to remove undesired atmospheric gaseous contaminants adsorbed on powder surface and/or pores. In some cases, powders were preliminary sonicated for 30 min in order to evaluate the presence (and stability) of particle aggregates. X-ray diffraction (XRD) patterns were obtained using a PW3040/60 X'Pert PRO MPD diffractometer by PANalytical equipped with a Cu Kα source, a Bragg−Brentano geometry in a flat or capillary sample-holder, and 10.240 s/step with 2θ steps of 0.01 in the 2θ range of 5−70°. The average crystallite size was estimated using the Scherrer equation. For the calculation, three diffraction peaks with the highest intensities were selected, and the reported size values were the average of the results obtained for each peak. High-resolution transmission electron microscopy (HRTEM) measurements were performed on a Jeol JEM 3010 UHR microscope (300 kV acceleration, LaB6 filament) equipped with a digital image acquisition GATAN (2k × 2k) and EDS microanalysis (Oxford INCA Energy Team 200). Thermal gravimetric and differential thermal analysis (TGA-DTA) was performed with a TA Instruments TGA Q600 unit. Sample treatments were carried out in flow of air or nitrogen, and the thermal program was stabilization at 40 °C, heating (in flow of air or nitrogen) at 500 or 800 °C using a ramp rate of 10 °C min^{-1}, maintaining at 500 or 800 °C for 10 min, and cooling to room temperature. Fourier transform infrared (FTIR) spectra were recorded on a Bruker IFS 88 transmission spectrophotometer equipped with a Globar source and DTGS detector. The resolution used was 4 cm^{-1} with 128 scans in the range of 4000−400 cm^{-1}. KBr pellets were used (sample concentration 5% w/w). Acid−base titrations were done with a Schott Titroline Alpha titrator equipped with a 20 mL burette syringe and connected to a Schott Blueline 11-pH glass combination electrode. The system was controlled using Pytrator software. The end points of the titration curves were determined from the maximum on the first derivative curve. The pK_a values were obtained from the minimum values of the first derivative of the pH curve. Reported results for each sample are the statistical average of at least three replicates. Particle size (d_z) and zeta potential (ζ) were measured on the aqueous dispersions of magnetite nanoparticles by laser doppler velocimetry coupled with photon correlation spectroscopy using a Coulter DELSA 440 spectrometer equipped with a 5 mW He−Ne laser (632.8 nm). Hydrodynamic diameters were deduced using the Stokes−Einstein equation and employing the particle diffusion coefficients calculated from the Doppler shift arising from Brownian motion. The electrophoretic mobility was calculated from the measurement of the Doppler shift for particles subjected to an electric field, and these data were further converted to ζ using the Smoluchowski equation.[23] All measurements were run in duplicate.

Sorption Experiments. To evaluate the adsorption ability of SBO-bonded Fe_3O_4 nanoparticles, the adsorption of crystal violet (CV) was investigated in aqueous solutions at 25 ± 0.2 °C. In a typical removal procedure, SBO-coated Fe_3O_4 nanoparticles were added into 200 mL of CV solution (10 mg L^{-1}). The concentrations of the NPs ranged from 0.1 to 2 g. The solution pH was adjusted by NaOH or HCl to the desired value. The mixture was stirred in a closed beaker for 3 h. Then the magnetic nanoparticles with sorbed CV were separated from the mixture with a permanent hand-held magnet. The residual CV concentration in the solution was determined spectrophotometrically using a double-beam Shimadzu UV/vis spectrophotometer. The effect of pH on the shape of the spectra was examined to avoid a misinterpretation of the spectrophotometric determinations at different pHs. For achieving the adsorption isotherms of CV, solutions with various initial dye concentrations were treated with the same procedure as above at room temperature

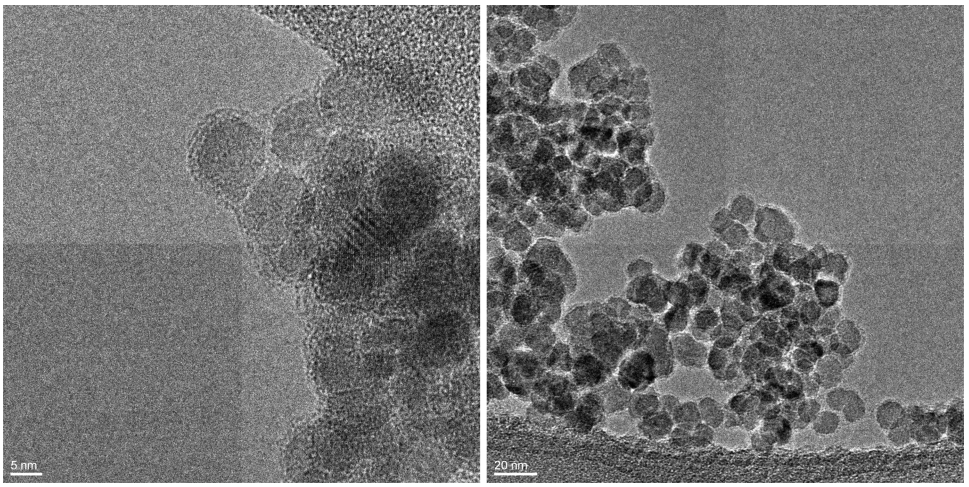

Figure 1. HR-TEM images of NP/0.5.

(25 ± 0.2 °C). Every experiment was performed in triplicate, and average values were used in the graphs.

In this study, all safety and environmental considerations have been taken into account. The chemical residues were disposed for further processing.

RESULTS AND DISCUSSION

Morphology and Structure. Figure 1 shows representative TEM images of the nanoparticles NP/0.5 dispersed in an aqueous medium. The particles appeared to be roughly spherical in shape, with a crystalline core and an external layer of organic matter. No significant differences were observed among the samples with different amounts of SBO (data not shown), except for the presence of the amorphous layer around the particles, which is never visible for samples NP/0.1 and NP/0.05. The analysis of the TEM images revealed an average particle size of 10.2 ± 1.7 nm (Figures S1, Supporting Information). This value is slightly larger than that previously reported using humic acids as the coating agent.[24] Formation of aggregates with no uniform size is also observed in the TEM images.

The analyses of all the interference patterns visible in the recorded images (more than 50 patterns were examined) agree in evidencing the presence of magnetite in orthorhombic form (d_{hkl} = 4.48 and 2.97 relative to (212) and (400) planes, which are the most common interplanar distances found; reference code 01-076-0955). Some of the patterns can be also assigned to the maghemite phase. It is the case of d_{hkl} = 4.29, 3.73, 2.78, and 2.51 relative to (105), (203), (216), and (119) planes of maghemite (reference code: 00-025-1402), but the same patterns can be assigned with almost good agreement to planes (220), (222), (314), (216), respectively, of orthorhombic magnetite phase.

The XRD pattern was used to identify the iron oxide phases of all the samples obtained from solutions of different SBO concentration (Figure S2, Supporting Information). All the peak positions at 30.1 (220), 35.4 (311), 43.0 (400), 53.9 (422) 57.2 (511), and 62.6 (440) are consistent with the standard X-ray data for the magnetite phase (card number 11-0614, ICCD Database). The small signal evidenced at 2θ = 44.6 could be assigned to a small amount of ferrite phase (110 plane, card number 6-0696), whose formation could occur randomly during the synthetic procedure. We did not observe any other iron oxide peaks in the diffraction pattern of the samples. For the calculus of the particle size, the diffraction peaks corresponding to (311), (511), and (440) magnetite planes were used. The average particle diameter estimated using the Scherrer formula for each sample was 12.2 ± 0.2 nm (NP/0.05), 12.2 ± 0.3 nm (NP/0.1), and 10.7 ± 1.0 nm (NP/0.5). These results show that the concentration of SBO employed in the synthesis does not significantly affect the size of the nanoparticles, which is in agreement with TEM measurements. Also, the particle sizes estimated by the Scherrer equation are quite close to the TEM results (see above), indicating that the cores of the nanoparticles are formed by single crystals.

To evaluate the thermal stability of the magnetite in the NPs, XRD diffraction patterns were recorded on NP/0.5, NP/0.1, and NP/0.05 samples previously heated to 800 °C under N_2 atmosphere (Figure S3, Supporting Information). These analyses revealed that the magnetite was almost completely converted into hematite after the thermal treatment in the NP/0.05 and NP/0.1 samples. However, for NP/0.5, magnetite and wüstite (FeO) were identified as crystal structures in the NPs. These results indicate that the amount of SBO used in the synthesis plays an important role in the thermal stability of the magnetic NPs.

The FTIR spectra of the SBO, bare Fe_3O_4 nanoparticles, and magnetic nanoparticles with different amounts of SBO are shown in Figure S4 of the Supporting Information. Magnetite was observed in the nanoparticle samples by a strong absorption at 561 and 617 cm^{-1}, which corresponds to the Fe−O stretching vibration.[16] The bands in the range from 1700 to 1300 cm^{-1} were mainly due to the stretching of carboxylic groups, while those at 1031 and 1109 cm^{-1} indicated C−O stretching of polysaccharides or polysaccharide-like substances.[25,26] Significant differences in the spectra bands related to carboxylic and carboxylate groups were observed between the free SBO and NPs samples. These differences are consistent with the carboxylate anions interacting with the FeO surface.[27] Moreover, a strong and pointed peak at 1400 cm^{-1} observed for the NPs samples is consistent with a carboxylate−iron stretching reported by Ou et al.[25] The band at 1113 cm^{-1} that appears in the SBO-coated NPs is a typical band of organic matter adsorbed on iron oxide, which is attributed to the adsorbed carbohydrates or polysaccharide-like substances.[27] No significant differences in the FTIR spectra were observed among the three samples of NPs.

Figure S5 of the Supporting Information shows the TGA curves obtained for the three samples of NPs synthesized with different amounts of SBO. The first weight loss (up to 150 °C) is assigned to adsorbed water elimination, while the second loss (up to 450 °C) is assigned to the thermal decomposition of organic matter attached to the NPs (see Table 1 for the % of organic matter bonded to the NPs measured for each sample). For the NP/0.05 and NP/0.1 samples, a third phenomenon occurs at about 600 °C. The formation of the peaks in the range of 550−650 °C in the DTA analysis for the NP/0.05 and NP/0.1 samples (inset of Figure S5, Supporting Information) allows us to assign the third step to the phase change of magnetite into hematite. These results are consistent with the XRD patterns of the samples heated to 800 °C (see above). Table 1 also reports the results obtained from the isotherms of N_2 adsorption at 77 K for NP/0.05, NP/0.1, and NP/0.5 (Figure S6, Supporting Information).

Table 1. Apparent Specific Surface Areas and SBO Amounts Bonded to the NPs Surfaces

sample	specific surface area[a] (m^2 g^{-1})	SBO adsorbed to Fe_3O_4[b] (%)
NP/0.5	35	~15
NP/0.1	55	~10
NP/0.05	63	~5

[a]BET model. [b]TGA analysis.

Figure 2A and B show the zeta potentials (ζ) and the particle sizes (d_z) of the bare and SBO-bonded Fe_3O_4 nanoparticles (125 mg L^{-1}) measured in 10^{-2} M KCl aqueous solutions at different pHs (3−12, adjusted with KOH or HCl). The pH of zero point charge (pH_{PZC}) of Fe_3O_4 was 7.2, which is close to that reported in the literature.[28] The pH_{PZC} of NP/0.05 and NP/0.5 decreased to the values of 6.8 and 3.0, respectively. Because SBO is negatively charged in the range of pH 3−12, the positive charge observed for NP/0.05 at pHs lower than 6.8 could be the consequence of the limited covering of the Fe_3O_4 surface by organic matter. However, when higher amounts of SBO are used (i.e., NP/0.5), a negative charge on the surface of the nanoparticles is observed over all the investigated pH values (3−12), which benefits the sorption of positively charged pollutants. Also, as shown in Figure 2A, ζ becomes more negative as the pH increases because of the dissociation of carboxylic and phenolic groups (see below). On the other hand, the pH dependence of d_z clearly shows for the three samples a maximum value of 1300 nm at pH_{PZC}, which decreases to a value of about 400 nm. Over the pH range between 6 and 9, the NP/0.5 sample presents the lower apparent size, incrementing its surface area for the adsorption of pollutants.

Carboxylic (−COOH) and phenolic (−OH) functional groups contents measured by titration and their respective apparent pK_a values for free SBO and the different NPs samples are shown in Table 2. The value 1.80 of the ratio −COOH/−OH obtained for this SBO is similar to that found for other types of SBO[12] and is lower than the reported 3.2 for commercial humic acids.[29,30] Although both carboxylic and phenolic groups may have complex Fe ions, the smaller −COOH/−OH ratio found for NPs (0.13 ± 0.03) suggests that a significant fraction of the carboxylic groups of the SBO may be bonded to the magnetite surface, as is also supported by the lower content of the COOH groups. A similar result was found for the binding of humic acids to magnetite nanoparticles.[24] On the other hand, both carboxylic and phenolic

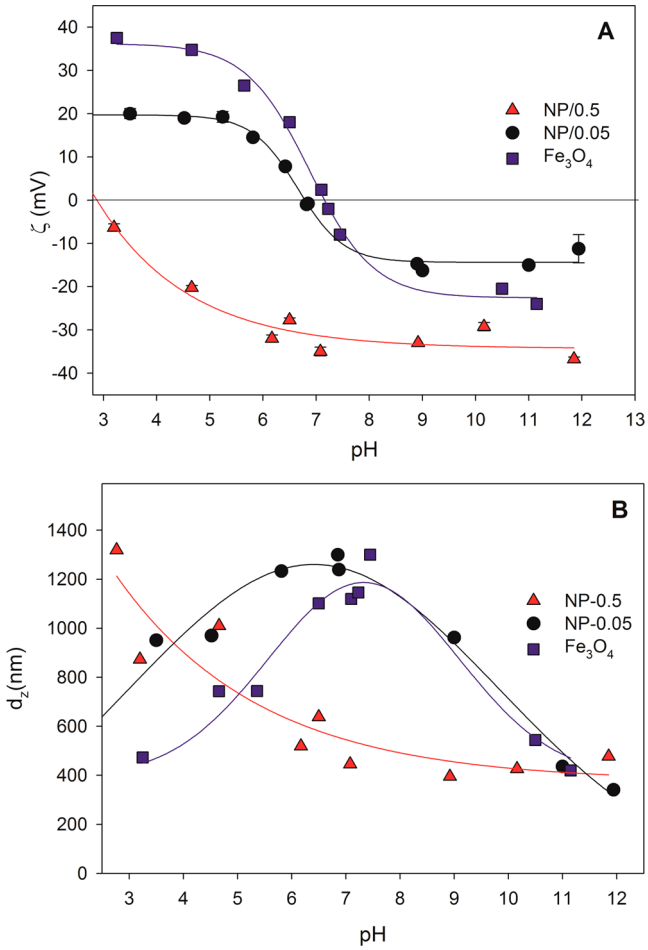

Figure 2. Variation of (A) zeta potentials (ζ) and (B) the particle sizes (d_z) of bare magnetite (Fe_3O_4), NP/0.05, and NP/0.5 as a function of pH in 0.01 M KCl.

groups contents increase with the amount of SBO used in the synthesis. The higher values of phenolic group contents found in the NPs samples compared to free SBO indicate that during the synthesis of the NPs the SBO undergoes a chemical process in which the SBO is hydroxylated by the oxidizing medium (pH ~ 12 and 90 °C). The lower phenolic pK_a values of the SBO bonded to the magnetite nanoparticles can be explained by the incorporation of hydroxyl groups in the aromatic rings during the synthesis procedure. The resulting polyhydroxylated phenols are more acidic than the monohydroxylated phenols due to resonance stabilization of the negative charge of the unprotonated species.[31]

Figure 3A reports the magnetization curves obtained for the three NPs. At 300 K, all samples exhibited superparamagnetic characteristics, including zero coercivity and remanence. The saturation magnetization (M_s) of the magnetite nanoparticles synthesized with different amounts of SBO were 67 (NP/0.05), 65 (NP/0.1), and 51 (NP/0.5) emu g^{-1}. This trend is consistent with the different amounts of magnetite per gram of sample (i.e., 0.95, 0.90, and 0.85 for NP/0.05, NP/0.1, and NP/0.5, respectively). Also, the decrease in M_s for all the samples compared to the bulk magnetite (92 emu g^{-1}) is often observed with the nanoparticles and is most likely attributed to the existence of organic coating agents.[32] Some studies suggested that the presence of the coating agents decreases the uniformity due to quenching of surface moments, resulting in the

dx.doi.org/10.1021/sc500213j | ACS Sustainable Chem. Eng. 2014, 2, 1518−1524

Table 2. Mean Concentration Values of Groups with Apparent pK_a on the Acid Side (Carboxylic Groups) and with pK_a on the Basic Side (Phenol Groups)[a]

sample	−COOH (mmol g^{-1})	pK_{a1}	Ph−OH (mmol g^{-1})	pK_{a2}	total acidity (mmol g^{-1})
SBO	1.40 ± 0.20	6.6 ± 0.1	0.78 ± 0.07	10.2 ± 0.1	2.1 ± 0.2
NP/0.05	0.13 ± 0.11	6.3 ± 0.3	0.91 ± 0.09	9.3 ± 0.2	1.0 ± 0.2
NP/0.1	0.21 ± 0.15	6.3 ± 0.1	1.3 ± 0.4	9.2 ± 0.1	1.5 ± 0.6
NP/0.5	0.25 ± 0.18	6.5 ± 0.1	2.8 ± 0.1	9.2 ± 0.1	3.0 ± 0.3

[a]Confidence interval between replicates of 95%.

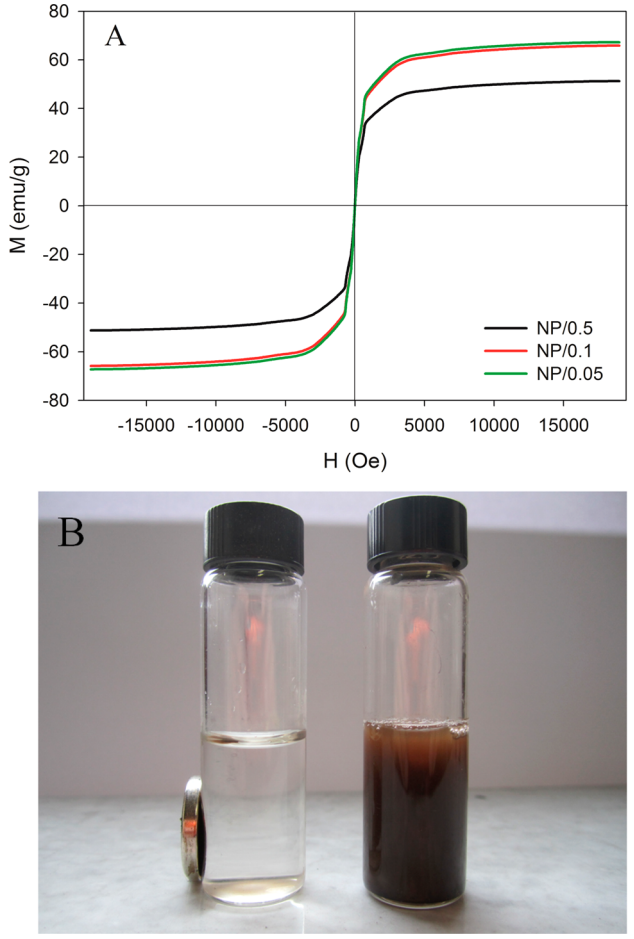

Figure 3. (A) Magnetization curves of NP/0.5, NP/0.1, and NP/0.05 at 300 K. (B) NP/0.5 dispersed in aqueous solution and magnetic separation.

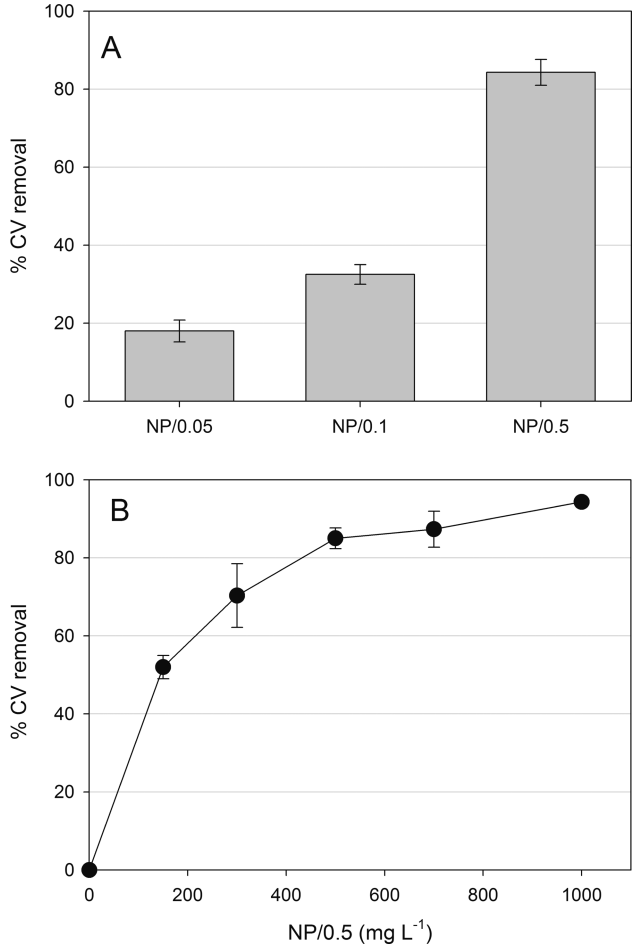

Figure 4. (A) CV removal obtained with NPs prepared with different amounts of SBO. $[CV]_0$ = 10 mg L^{-1}; $[NP]_0$ = 500 mg L^{-1}; pH = 7, T = 25 ± 2 °C. (B) Effect of NP/0.5 dosage on the adsorption of CV. $[CV]_0$ = 10 mg/L, pH = 7, T = 25 ± 2 °C. The error bars represent the standard deviation of the data obtained by triplicate.

reduction of magnetic moments in such nanoparticles.[33] Although higher amounts of SBO (higher covering) decrease the M_s values of the NPs, for the three samples, the separation of the NPs from its aqueous dispersions can be easily completed in a few minutes with permanent hand-held magnets (Figure 3B). The dried samples are magnetically stable for a very long period of time (they were monitored for a period of 2.5 years); in water suspension form, they are stable for a period of at least 6 months.

Application of NPs as Nanoadsorbent for Crystal Violet Removal. Crystal violet (CV) was used to evaluate the adsorption capacity of the NPs. Sorption took place rapidly, within the first 30 min, but to be sure to reach sorption equilibrium, the samples were taken for 3 h in contact with CV. The effect of the three different adsorbents on the CV removal at neutral pH was evaluated (Figure 4A). The highest % CV removal was found for the NP/0.5 (about 85%) as expected considering the zeta potential measurements (Figure 2A), i.e., the high negative charge measured at the surface of the NP/0.5 at pH 7 favors sorption of the cationic dye. Figure 4B shows the increase in the adsorption capacity of NP/0.5 with increasing concentration of the adsorbent up to a CV removal of 95% at 1000 mg L^{-1}.

The equilibrium isotherms for the adsorption of CV on NP/0.5 at pH 7 and 25 °C are shown in Figure 5 for adsorbent concentrations of 150 and 1000 mg L^{-1}. Under both conditions, the adsorption data were fitted by the Freundlich sorption model (eq 1 reported in linearized form).

$$\log Q_e = \log K_f + (1/n)\log C_e \quad (1)$$

dx.doi.org/10.1021/sc500213j | ACS Sustainable Chem. Eng. 2014, 2, 1518−1524

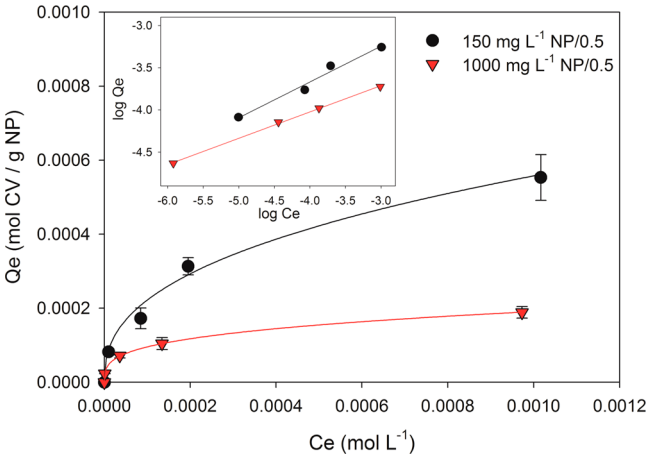

Figure 5. Adsorption isotherms of CV on NP/0.5 obtained at pH = 7 and 25 ± 2 °C with different NP/0.5 concentrations (150 mg L^{-1} and 1000 mg L^{-1}). The error bars represent the standard deviation of the data obtained by triplicate. Inset: Logarithmic plot of the data according to the Freundlich linearized model (eq 1).

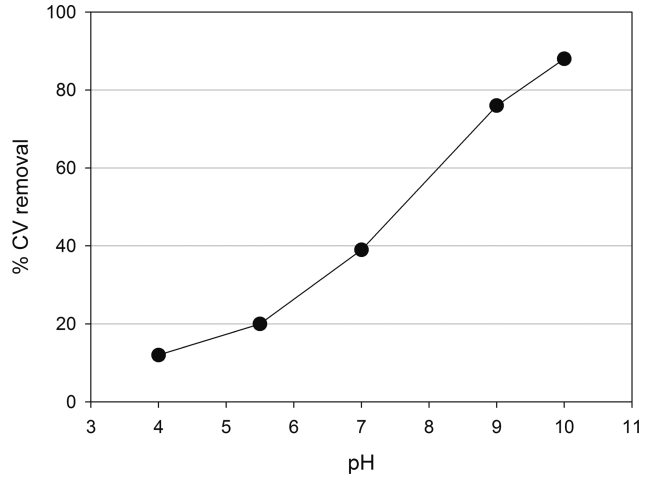

Figure 6. CV removal obtained with NP/0.5 at different pHs. $[CV]_0$ = 10 mg L^{-1}; $[NP/0.5]_0$ = 150 mg L^{-1}.

where Q_e is the sorbed CV concentration on the solid (mol g^{-1}), C_e is the equilibrium CV concentration (mol L^{-1}), and K_f and n are constants at a given temperature. The value of K_f is indicative of the affinity adsorptive/adsorbent and $1/n$ is an experimentally determined constant. Fitting our data to eq 1 yielded in both cases linear relationships with R^2 greater than 0.98 (inset of Figure 5). Freundlich parameters for sorption (K_f and n) calculated from the slope and intercept of the linear regression are listed in Table S1 of the Supporting Information. The difference observed in the Freundlich parameters at low and high concentrations of NP/0.5 can be assigned to the higher aggregation of the nanoparticles expected for the 1000 mg/L series of experiments. There is no contradiction between this result and those obtained from Figure 4B because the isotherms reflect the amount of CV adsorbed per gram of NPs. Aggregation causes a decrease in the active surface area of the adsorbent and thus seems to be a significant parameter that rules out the sorption capacity of the dye. Similar observations have been made with iron-containing hydroxyapatite nanoparticles used for the removal of Cu^{2+}.[34]

The effect of medium pH on CV removal with NP/0.5 was studied by performing sorption experiments over the pH range of 3−10. Values of pH higher than 10 were not studied to avoid hydrolysis of CV.[35] The sorption of CV on the surface of NP/0.5 is significantly influenced by pH (Figure 6). The % CV removal increases as the pH increases up to pH 10 in agreement with the change of ζ and d_z with pH. On the other hand, the ionic strength effect on the sorption of CV was evaluated by the addition of different amounts of NaCl. Experiments performed at pH 7, with $[CV]_0$ = 10 mg L^{-1}, $[NP/0.5]_0$ = 150 mg L^{-1}, and $[NaCl]_0$ = 0.005−0.1 M, showed that the sorption of CV is not affected by the presence of NaCl (data not shown). Evidently, CV exhibits greater selectivity toward the sorbent and is not displaced by the salt, and the addition of NaCl under the tested conditions do not affect significantly the aggregation of the NPs, which is important for applications to real wastewaters. Similar results were obtained by Janos,[36] who studied the cationic dyes removal with iron humate.

We clearly demonstrate that SBO, a biobased product isolated from urban solid wastes, can be easily transformed into a low-cost magnetic nanoadsorbent employing a simple coprecipitation method. Further research on the adsorption of other variety of pollutants (e.g., heavy metals) and the recyclability of these NPs is still needed in order to evaluate the potential of this material for large-scale removal of pollutants from wastewaters.

■ ASSOCIATED CONTENT

Supporting Information

Figures S1−S6 and Table S1. This material is available free of charge via the Internet at http://pubs.acs.org.

■ AUTHOR INFORMATION

Corresponding Author

*Phone: +54 221 4257430. Fax: +54 221 4254642. E-mail: lcarlos@quimica.unlp.edu.ar. Address: Casilla de correo 16, sucursal 4 (1900), La Plata, Argentina.

Present Address

E. Montoneri: University of Foggia, STAR*Integrated Research Unit, Via Gramsci, 89-91, Foggia, Italy.

Notes

The authors declare no competing financial interest.

■ ACKNOWLEDGMENTS

This research was supported by ANPCyT, Argentina (PICT 2008 No. 00686), CONICET, and CICPBA, Argentina, by the European Union (PIRSES-GA-2010-269128, EnvironBOS) and Ministero delle Politiche Agricole e Forestali for the Agrienergia project. The authors are also thankful to the following institutions: Acea Pinerolese Spa in Pinerolo (TO) for supplying the biobased substances sourcing materials and Studio Chiono ed Associati in Rivarolo Canavese (TO) for making available pilot equipment and services for the production of the biobased substances. L.G.G., M.C.G., and L.C. are researchers from CONICET. D.O.M. is a researcher from CICPBA.

■ REFERENCES

(1) Tong, D. S.; Zhou, C. H.; Lu, Y.; Yu, H.; Zhang, G. F.; Yu, W. H. Adsorption of acid red G dye on octadecyl trimethylammonium montmorillonite. *Appl. Clay Sci.* **2010**, *50*, 427−431.

(2) Ghorai, S.; Sarkar, A. K.; Panda, A. B.; Pal, S. Effective removal of Congo red dye from aqueous solution using modified xanthan gum/

silica hybrid nanocomposite as adsorbent. *Bioresour. Technol.* **2013**, *144*, 485−491.
(3) Bailey, S. E.; Olin, T. J.; Bricka, R. M.; Adrian, D. D. A review of potentially low-cost sorbents for heavy metals. *Water Res.* **1999**, *33*, 2469−2479.
(4) Lim, A. P.; Aris, A. Z. A review on economically adsorbents on heavy metals removal in water and wastewater. *Rev. Environ. Sci. Biotechnol.* **2013**, 1−19.
(5) Crini, G. Non-conventional low-cost adsorbents for dye removal: A review. *Bioresour. Technol.* **2006**, *97*, 1061−1085.
(6) Wan Ngah, W. S.; Hanafiah, M. A. K. M. Removal of heavy metal ions from wastewater by chemically modified plant wastes as adsorbents: A review. *Bioresour. Technol.* **2008**, *99*, 3935−3948.
(7) Putra, E. K.; Pranowo, R.; Sunarso, J.; Indraswati, N.; Ismadji, S. Performance of activated carbon and bentonite for adsorption of amoxicillin from wastewater: Mechanisms, isotherms and kinetics. *Water Res.* **2009**, *43*, 2419−2430.
(8) Khattri, S. D.; Singh, M. K. Removal of malachite green from dye wastewater using neem sawdust by adsorption. *J. Hazard. Mater.* **2009**, *167*, 1089−1094.
(9) Avetta, P.; Bella, F.; Bianco Prevot, A.; Laurenti, E.; Montoneri, E.; Arques, A.; Carlos, L. Waste cleaning waste: Photodegradation of monochlorophenols in the presence of waste-derived photosensitizer. *ACS Sustainable Chem. Eng.* **2013**, *1*, 1545−1550.
(10) Boffa, V.; Perrone, D. G.; Montoneri, E.; Magnacca, G.; Bertinetti, L.; Garlasco, L.; Mendichi, R. A waste-derived biosurfactant for the preparation of templated silica powders. *ChemSusChem* **2010**, *3*, 445−452.
(11) Magnacca, G.; Laurenti, E.; Vigna, E.; Franzoso, F.; Tomasso, L.; Montoneri, E.; Boffa, V. Refuse derived bio-organics and immobilized soybean peroxidase for green chemical technology. *Process Biochem.* **2012**, *47*, 2025−2031.
(12) Montoneri, E.; Boffa, V.; Savarino, P.; Perrone, D. G.; Musso, G.; Mendichi, R.; Chierotti, M. R.; Gobetto, R. Biosurfactants from urban green waste. *ChemSusChem* **2009**, *2*, 239−247.
(13) Gomis, J.; Bianco Prevot, A.; Montoneri, E.; González, M. C.; Amat, A. M.; Mártire, D. O.; Arques, A.; Carlos, L. Waste sourced bio-based substances for solar-driven wastewater remediation: Photo-degradation of emerging pollutants. *Chem. Eng. J.* **2014**, *235*, 236−243.
(14) Carlos, L.; García Einschlag, F. S.; González, M. C.; Mártire, M. O. In *Waste Water − Treatment Technologies and Recent Analytical Developments*; García Einschlag, F. S., Ed.; InTech: Rijeka, Croatia, 2013; ISBN: 978-953-51-0882-5.
(15) Montoneri, E.; Mainero, D.; Boffa, V.; Perrone, D. G.; Montoneri, C. Biochemenergy: A project to turn an urban wastes treatment plant into biorefinery for the production of energy, chemicals and consumer's products with friendly environmental impact. *Int. J. Global Environ. Issues* **2011**, *11*, 170−196.
(16) Maity, D.; Agrawal, D. C. Synthesis of iron oxide nanoparticles under oxidizing environment and their stabilization in aqueous and non-aqueous media. *J. Magn. Magn. Mater.* **2007**, *308*, 46−55.
(17) Panneerselvam, P.; Morad, N.; Tan, K. A. Magnetic nanoparticle (Fe_3O_4) impregnated onto tea waste for the removal of nickel(II) from aqueous solution. *J. Hazard. Mater.* **2011**, *186*, 160−168.
(18) Peng, L.; Qin, P.; Lei, M.; Zeng, Q.; Song, H.; Yang, J.; Shao, J.; Liao, B.; Gu, J. Modifying Fe_3O_4 nanoparticles with humic acid for removal of Rhodamine B in water. *J. Hazard. Mater.* **2012**, *209−210*, 193−198.
(19) Fan, L.; Luo, C.; Sun, M.; Li, X.; Lu, F.; Qiu, H. Preparation of novel magnetic chitosan/graphene oxide composite as effective adsorbents toward methylene blue. *Bioresour. Technol.* **2012**, *114*, 703−706.
(20) Asad, S.; Amoozegar, M. A.; Pourbabaee, A. A.; Sarbolouki, M. N.; Dastgheib, S. M. M. Decolorization of textile azo dyes by newly isolated halophilic and halotolerant bacteria. *Bioresour. Technol.* **2007**, *98*, 2082−2088.
(21) Au, W.; Pathak, S.; Collie, C. J.; Hsu, T. C. Cytogenetic toxicity of gentian violet and crystal violet on mammalian cells in vitro. *Mutat. Res.* **1978**, *58*, 269−276.
(22) Gomis, J.; Vercher, R. F.; Amat, A. M.; Mártire, D. O.; González, M. C.; Bianco Prevot, A.; Montoneri, E.; Arques, A.; Carlos, L. Application of soluble bio-organic substances (SBO) as photocatalysts for wastewater treatment: Sensitizing effect and photo-Fenton-like process. *Catal. Today* **2013**, *209*, 176−180.
(23) Hunter, R. J. Principles and Applications. In *Zeta Potential in Colloid Science*; Academic Press: London, 1988.
(24) Carlos, L.; Cipollone, M.; Soria, D. B.; Sergio Moreno, M.; Ogilby, P. R.; García Einschlag, F. S.; Mártire, D. O. The effect of humic acid binding to magnetite nanoparticles on the photogeneration of reactive oxygen species. *Sep. Purif. Technol.* **2012**, *91*, 23−29.
(25) Ou, X.; Chen, S.; Quan, X.; Zhao, H. Photochemical activity and characterization of the complex of humic acids with iron(III). *J. Geochem. Explor.* **2009**, *102*, 49−55.
(26) Celi, L.; Lamacchia, S.; Marsan, F. A.; Barberis, E. Interaction of inositol hexaphosphate on clays: Adsorption and charging phenomena. *Soil Science* **1999**, *164*, 574−585.
(27) Gu, B.; Schmitt, J.; Chen, Z.; Liang, L.; McCarthy, J. F. Adsorption and desorption of natural organic matter on iron oxide: Mechanisms and models. *Environ. Sci. Technol.* **1994**, *28*, 38−46.
(28) Chang, Y. C.; Chen, D. H. Preparation and adsorption properties of monodisperse chitosan-bound Fe_3O_4 magnetic nano-particles for removal of Cu(II) ions. *J. Colloid Interface Sci.* **2005**, *283*, 446−451.
(29) Gao, K.; Pearce, J.; Jones, J.; Taylor, C. Interaction between peat, humic acid and aqueous metal ions. *Environ. Geochem. Health* **1999**, *21*, 13−26.
(30) Ritchie, J. D.; Michael Perdue, E. Proton-binding study of standard and reference fulvic acids, humic acids, and natural organic matter. *Geochim. Cosmochim. Acta* **2003**, *67*, 85−93.
(31) Mukherji, S. M.; Singh, S. P.; Kapoor, R. P.; Dass, R. *Organic Chemistry*, Vol. *II*; New Age International Publishers: New York, 2012.
(32) Sun, X.; Zheng, C.; Zhang, F.; Yang, Y.; Wu, G.; Yu, A.; Guan, N. Size-controlled synthesis of magnetite (Fe_3O_4) nanoparticles coated with glucose and gluconic acid from a single Fe(III) precursor by a sucrose bifunctional hydrothermal method. *J. Phys. Chem. C* **2009**, *113*, 16002−16008.
(33) Kim, D. K.; Mikhaylova, M.; Zhang, Y.; Muhammed, M. Protective coating of superparamagnetic iron oxide nanoparticles. *Chem. Mater.* **2003**, *15*, 1617−1627.
(34) Mercado, D. F.; Magnacca, G.; Malandrino, M.; Rubert, A.; Montoneri, E.; Celi, L.; Bianco Prevot, A.; Gonzalez, M. C. Paramagnetic iron-doped hydroxyapatite nanoparticles with improved metal sorption properties. A bioorganic substrates-mediated synthesis. *ACS Appl. Mater. Interfaces* **2014**, *6*, 3937−3946.
(35) Arias-Estevez, M.; Astray, G.; Cid, A.; Fernández-Gándara, D.; García-Río, L.; Mejuto, J. C. Influence of colloid suspensions of humic acids upon the alkaline fading of carbocations. *J. Phys. Org. Chem.* **2008**, *21*, 555−560.
(36) Janoš, P. Sorption of basic dyes onto iron humate. *Environ. Sci. Technol.* **2003**, *37*, 5792−5798.